Atomic Resolution (0.98 Å) Structure of Eosinophil-Derived Neurotoxin[†,‡]

G. Jawahar Swaminathan,[§] Daniel E. Holloway,[§] Kasinadar Veluraja,[§,||] and K. Ravi Acharya*[,§]

Department of Biology and Biochemistry, University of Bath, Claverton Down, Bath BA2 7AY, U.K.

Received November 1, 2001; Revised Manuscript Received December 10, 2001

ABSTRACT: Human eosinophil-derived neurotoxin (EDN) is a small, basic protein that belongs to the ribonuclease A superfamily. EDN displays antiviral activity and causes the neurotoxic Gordon phenomenon when injected into rabbits. Although EDN and ribonuclease A have appreciable structural similarity and a conserved catalytic triad, their peripheral substrate-binding sites are not conserved. The crystal structure of recombinant EDN (rEDN) has been determined at 0.98 Å resolution from data collected at a low temperature (100 K). We have refined the crystallographic model of the structure using anisotropic displacement parameters to a conventional R-factor of 0.116. This represents the highest resolution structure of rEDN determined to date and is only the second ribonuclease structure to be determined at a resolution greater than 1.0 Å. The structure provides a detailed picture of the conformational freedom at the various subsites of rEDN, and the water structure accounts for more than 50% of the total solvent content of the unit cell. This information will be crucial for the design of tight-binding inhibitors to restrain the ribonucleolytic activity of rEDN.

The eosinophil-derived neurotoxin (EDN)[1] is a small, basic protein that belongs to the ribonuclease A (RNase A; EC 3.1.27.5) superfamily (*1*, *2*). It is predominantly localized to the matrix of large secretory granules in eosinophils (*3*) and is also known as RNase-2, nonsecretory RNase, and RNase-U_s, the latter on the basis of its specificity toward uridine-containing nucleotides (*4*). Because eosinophilic leukocytes are considered by some to be involved in host−parasite defense mechanisms, a role for EDN as a host defense protein has been suggested (*5*). However, EDN exhibits very weak toxicity toward helminth parasites (*6*), although it is considerably more effective against single-stranded RNA viruses (*7*). The initial identification of EDN was based on its ability to cause the Gordon phenomenon when injected into rabbits intrathecally (*8*−*10*). This response is characterized by ataxia, incoordination, spasmodic paralysis, and muscle stiffness and appears to be related to selective killing of cerebellar Purkinje cells by EDN (*11*). Other related ribonucleases, namely, eosinophil cationic protein (ECP) (*8*, *12*) and Onconase (*13*), also demonstrate neurotoxic activity.

Although EDN shares 67% amino acid sequence identity with ECP, its sequence identity with RNase A is only 36%. The ribonucleolytic activity of EDN is also between 3- and 30-fold lower than that of RNase A, depending on the substrate used (*14*, *15*). Nevertheless, this enzymatic activity is a prerequisite for its cytotoxic, neurotoxic, and antiviral activities (*7*, *13*, *14*). The primary sequence of EDN contains a Trp-X-X-Trp motif between residues 7 and 10, specifying an unusual C-mannosylation of Trp7. This involves the attachment of an α-mannosyl residue via a C−C link to the indole moiety of Trp7 and was the first example of this particular post-translational modification to be reported (*16*, *17*).

The crystal structure of recombinant EDN (rEDN) has previously been determined in complex with sulfate at 1.83 Å resolution (*18*) and with different adenylic mononucleotide inhibitors at comparable resolutions (*19*). Although EDN and RNase A share a common core catalytic site (Figure 1), there are significant differences at the peripheral substrate-binding subsites that could contribute to the differences in enzymatic activity observed between these two proteins (*20*). The identification and classification of these subsites are based on structural, mutational, and kinetic studies conducted on RNase A in the presence of various nucleotide-based inhibitors (for recent reviews, see refs *21*, *22*). The central subsites of the active site are designated B_1, P_1, and B_2, and these subsites accommodate the phosphate ester linkage where cleavage occurs (at P_1) and the nucleotide bases upstream (5′) and downstream (3′) of the scissile bond (at B_1 and B_2, respectively). Ribonucleases contain three invariant residues at the P_1 site that are maintained in EDN as His15, Lys38, and His129. The key B_1 residues in RNase A, Thr45 and Phe120, are also preserved in EDN as Thr42 and Leu130. However, subsite B_2 and the peripheral P_0 and P_2 subsites of RNase A (*23*−*26*) are not conserved in EDN. In addition, a new subsite, hitherto not seen in other ribonucleases, was identified in the EDN-sulfate complex and designated as P_{-1} (*18*). These differences in substrate-

[†] This work was supported by the Medical Research Council (U.K.) (Program Grant 9540039), a Royal Society-Leverhulme Trust (U.K.) Senior Research Fellowship to K.R.A, and a Royal Society (U.K.) and Indian National Science Academy (India) Short-Term Visiting Fellowship to K.V.

[‡] The atomic coordinates of rEDN have been deposited with the RCSB Protein Data Bank (accession code 1GQV).

* To whom correspondence should be addressed. Phone: 44-1225-826 238. Fax: 44-1225-826 779. E-mail: K.R.Acharya@bath.ac.uk.

[§] Department of Biology and Biochemistry, University of Bath.

[||] Present address: Department of Physics, Manonmaniam Sundaranar University, Tirunelveli 627 002, India.

[1] Abbreviations: EDN, eosinophil-derived neurotoxin; rEDN, recombinant EDN; ECP, eosinophil cationic protein; 5′-ADP, adenosine-5′-diphosphate; rmsd, root-mean-square deviation.

10.1021/bi015911f CCC: $22.00
Published on Web 02/13/2002

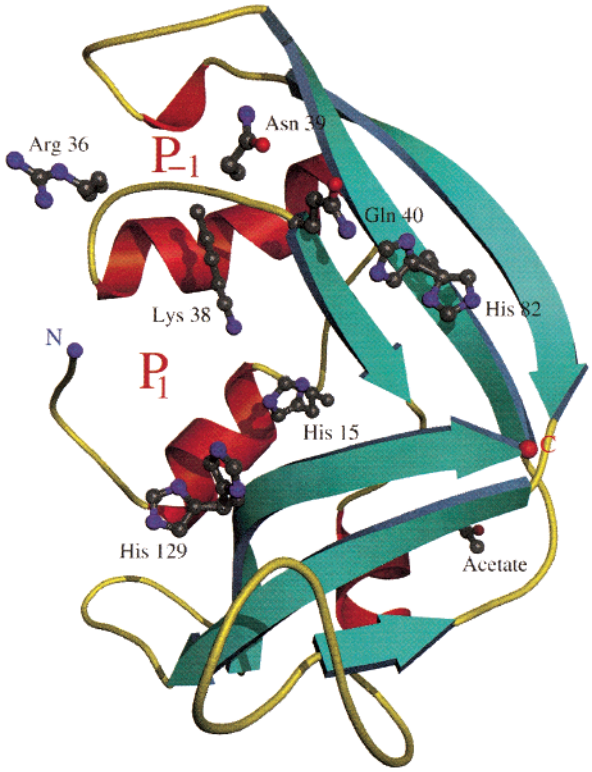

FIGURE 1: Ribbon representation of the rEDN molecule determined at 0.98 Å resolution. Subsite P_1 (His15, Lys38, and His129), subsite P_{-1} (Arg36, Asn39, and Gln40), and His82 from the vicinity of the B_1 subsite are shown in ball-and-stick representation. The N and C termini are shown as blue and red spheres, respectively, and the single acetate ion in the structure is indicated.

binding site organization are likely to give rise to the subtle differences in the substrate specificities of EDN and RNase A. Both EDN and RNase A bind pyrimidines at B_1 and prefer purines at B_2, but EDN has a 2-fold preference for cytidine over uridine and a 100-fold preference for adenosine at B_2 with dinucleotide substrates (*14*). The substrate specificities for RNase A at B_1 are similar to that seen for EDN, but the preference for adenosine at B_2 with dinucleotide substrates is more marked than in EDN (*27*, *28*).

The study of a protein at atomic resolution (better than 1.2 Å) provides a highly detailed model of that protein. At such a resolution, features that are not usually discernible at lower resolution, such as hydrogen positions and anisotropic motions of protein atoms, can be modeled (*29*). Atomic resolution structures also provide valuable information about solvent structure and various geometric and conformational properties of proteins (*30*) and serve to improve the library of stereochemical target values and validation of structures determined at lower resolution. Of the over 14 000 structures determined by X-ray crystallography and deposited in the Protein Data Bank (*31*), only 83 structures are at a resolution better than 1.0 Å with only 5 ribonuclease structures at a resolution better than 1.20 Å (*32*, *33*).

Here, we present the structure of rEDN at 0.98 Å resolution, determined from diffraction data collected under cryocooling conditions (100 K). This structure has the highest resolution of any EDN structure determined so far and provides insights into protein side-chain disorder and the conformational freedom of key residues involved in enzyme catalysis. The structure is described in detail with special attention paid to residues comprising the active site. This includes the P_{-1} subsite in the absence of any nucleotide inhibitor or polyvalent anion. The present results also suggest that residue His82, situated in the vicinity of the B_1 subsite, shows sulfate/pH-related conformational variation as seen for catalytic residue His129. Our results provide an improved map of the EDN active site residues and pave the way for the design of potent inhibitors that can be used to combat symptoms associated with EDN function.

EXPERIMENTAL PROCEDURES

Protein Purification and Crystallization. The expression of rEDN in *Escherichia coli* and purification protocols followed have been described previously (*19*). Crystals of rEDN were obtained at 16 °C using the hanging drop/vapor diffusion method. Drops containing 1.7 mg/mL rEDN, 0.05 M sodium cacodylate buffer (pH 6.5), and 0.7 M sodium acetate were suspended over reservoirs containing 0.1 M sodium cacodylate buffer (pH 6.5) and 1.4 M sodium acetate. Single crystals were obtained within 24 h. A cryoprotectant was prepared by adding glycerol to the mother liquor to a final concentration of 20% (v/v).

Data Collection. Diffraction data to a minimum Bragg spacing of 0.98 Å were collected from flash-cooled rEDN crystals using an ADSC Quantum-4 CCD detector at Protein Crystallography station PX 9.6 at the Synchrotron Radiation Source, Daresbury, U.K. To obtain a complete data set at this resolution, the following strategy was employed: 130 images with a 1° oscillation were collected at the highest resolution (0.98 Å) followed by a 60 images with a 1.5° oscillation per image at medium resolution (2 Å). A final low resolution pass (3.5 Å) of 50 images with a 2° oscillation per image filled low resolution shells. rEDN crystals belong to the space group $P2_12_12_1$ with cell dimensions of $a = 53.02$, $b = 57.48$, and $c = 42.40$ Å and have one molecule in the asymmetric unit. From the Wilson plot (*34*), an overall B-factor of 10.9 Å^2/Da was estimated. The overall completeness of the data was 99.6% with all but 310 reflections of the theoretical maximum recorded. In the highest resolution shell, data were 99.9% complete with just eight reflections not recorded. Of all the reflections in the highest resolution shell, over 80% of the reflections had $I/\sigma I > 3.0$, indicating that the diffraction limit of these crystals was beyond 0.98 Å. A summary of data processing is given in Table 1.

Refinement. Initial crystallographic refinement was carried out against 98.5% of the measured data using the program CNS (*35*). The remaining 1.5% (1031 reflections), which was randomly excluded from the full data set, was used for cross-validation by calculating the free R-factor (R-free) to follow the progress of refinement (*36*). The same subset of reflections was used throughout the refinement. The reference set was excluded from the calculation of electron density maps. In the final steps of refinement, all data were included.

The starting model for the refinement was derived from the previously submitted 1.6 Å resolution structure of rEDN in complex with sulfate ions (PDB entry 1HI2) (*19*) which contains 135 residues, 106 water molecules, and 2 sulfate ions located in the active site. All solvent molecules and anions were excluded to produce the starting model for refinement. Because the cell dimensions of the starting model

Table 1: Data Collection and Processing Statistics

wavelength	0.87 Å
resolution range (Å)	40−0.98
space group	$P2_12_12_1$
cell dimensions (Å)	a = 53.02, b = 57.48, c = 42.4
detector type	ADSC Quantum-4 CCD
no. of observations	614 353
unique reflections	74 763
R_{symm} (%)[a]	5.7
(outermost shell)[b]	(42.1)
completeness (%)	99.6
(outermost shell)[b]	(99.9)
$I/\sigma I$	21.7
(outermost shell)[b]	(3.7)
Matthews coeff (Å^3/Da)	1.96
solvent content (%)	36.8
Wilson B factor (Å^2)[c]	10.9

[a] $R_{symm} = \sum_h\sum_i[|I_i(h) - \langle I(h)\rangle|/\sum_h\sum_i I_i(h)]$, where I_i is the ith measurement and $\langle I(h)\rangle$ is the weighted mean of all measurements of $I(h)$. [b] Outermost shell is 1.02−0.98 Å. [c] Wilson B factor calculation performed using TRUNCATE (*63*).

were slightly different from the current data set, the CNS refinement protocol included an initial 40 cycles of rigid-body refinement. These were followed by consecutive cycles of energy minimization, isotropic B-factor minimization, and simulated annealing as implemented in CNS (*37*), interspersed with manual model building and analysis with O (*38*). The refinement in CNS was started at 1.6 Å resolution and gradually increased in subsequent rounds of refinement to a final resolution of 0.98 Å. Water molecules were incorporated into the structure at each step if they had peaks greater than 3σ in $F_o - F_c$ electron density maps and were within hydrogen-bond forming distances from appropriate atoms. A final refined model at 0.98 Å resolution, having an R-factor of 22.7% and R-free of 24.0%, with 133 water molecules and one acetate ion, was used for anisotropic refinement in SHELX-97 (*39*).

Initial conjugate gradient least-squares (CGLS) refinement was performed on the model produced by CNS using intensities rather than structure factor amplitudes with the same R-free subset as defined in CNS. The bond distances and angles (1,2 and 1,3 distances) were constrained using standard Engh and Huber restraints (*40*). Each cycle of refinement with SHELXL consisted of 10 cycles of restrained CGLS refinement followed by calculation and visualization of $2F_o - F_c$ and $F_o - F_c$ electron density maps and manual model rebuilding. Peaks predicted by the SHELXL program were inspected visually and included as water molecules or rejected based on the electron density maps. Initial rounds of restrained CGLS refinement were carried out by keeping all atomic displacement parameters (ADPs) isotropic. Subsequently, the ADPs were converted to anisotropic values, leading to improvements in the Fourier maps. Any alternate conformations seen in the electron density maps were added at this stage and refined isotropically for at least two rounds before being refined anisotropically. In each case, the site occupancy factors (SOFs) were refined such that their sum was unity. The occupancy of disordered water molecules was fixed at 1.0 or 0.5, depending on electron density peak height. The bulk solvent was modeled using Babinet's principle, as implemented in the SWAT option in SHELXL. At the beginning of SHELXL refinement, default values were used for all distances, planarity, chiral, and antibumping restraints (standard deviations were 0.02 Å for 1,2 distances, 0.04 Å for 1,3 distances, 0.2 Å^3 for chiral volumes and flat planes, and 0.02 Å for antibumping restraints). However, by the end of refinement, these restraints were relaxed by increasing standard deviations of the 1,2 distances, 1,3 distances and antibumping restraints to 0.03, 0.06, and 0.04 Å, respectively. The restraint defining planarity for the peptide bond was removed during final cycles of refinement after an initial starting standard deviation of 0.5 Å^3 was applied. Restraints that define the U_{ij} components of bonded atoms (DELU restraint) were applied with a standard deviation of 0.01 Å^2. Corresponding U_{ij} components of spatially adjacent atoms were weakly restrained to be the same with a standard deviation of 0.01 Å^2 (SIMU). However, these restraints on the ADPs were relaxed to final standard deviations of 0.02 and 0.04 Å^2 by the end of refinement. The ISOR restraint applied to the ADPs of solvent atoms to approximate isotropic behavior was kept at 0.1 Å^2.

The final round of refinement was carried out with the addition of riding hydrogen atoms at their calculated positions for protein residues alone, excluding alternate conformers of amino acid residues. The flexible loop region corresponding to residues 88−95 is poorly ordered in all rEDN structures, including the structure described here. This region was refined isotropically throughout the refinement process. The positions of hydrogen atoms were not refined but instead were calculated based on established geometrical criteria. The final R factor for the structure was 11.59%. Detailed statistics for refinement are given in Table 2.

RESULTS

Refinement Procedure. The structure of rEDN was initially refined using CNS v1.0 (*35*). Isotropic refinement was carried out in small steps starting at the resolution of the starting model (1.6 Å) with a gradual increase in resolution at each step until maximum resolution was reached. Isotropic refinement converged to an R factor of 22.7% and R-free of 24.0% after inclusion of 133 water molecules and 1 acetate ion from the crystallization medium. Subsequent isotropic refinement was carried out using SHELX-97 (*39*) using data to the highest possible resolution. Isotropic refinement reached a residual R-factor of 19.0% before anisotropic refinement of the structure was carried out (anisotropic refinement of the B-factors was vindicated by the reasonably high reflection-to-parameter ratio of 5.9). The switch from isotropic to anisotropic refinement resulted in a dramatic drop in R-factor to 13.9% (ΔR = 5.1%) accompanied by a 5−6% decrease in R-free. Many hydrogen atoms were visible in the electron density maps at this stage, particularly in residues involved in main-chain hydrogen bonds (Figure 2a). At this stage, alternate conformations were built into the model by reference to $2F_o - F_c$ and $F_o - F_c$ electron density maps. The occupancies of these alternate conformations were only refined isotropically. Water molecules were included in each cycle of the refinement process with occupancies fixed to 1.0 or 0.5 according to their electron density level in the maps. A region corresponding to residues 89−95 was highly disordered with poor electron density for the main chain; these residues were only refined isotropically throughout the refinement procedure. In the final steps of refinement, riding hydrogens were added to the model, excepting any associated with solvent ions, partial conformations, or regions of high disorder. Restraints were appropriately adjusted to provide

Table 2: Refinement Parameters and Statistics of the Final Model

resolution (Å)	0.98
no. of residues	135
R factor for all data (%)[a]	11.59
R factor for $F > 4\sigma$ (%)	11.02
R-free (%)[b]	14.44
Number of Non-H Atoms	
protein	1166
water	226
others	4
no. of observations per parameter[c]	5.93
goodness of fit	2.314

Deviations from Ideality geometry	rmsd	target σ
bond distances (Å)[d]	0.012	0.030
angle distances (Å)[d]	0.034	0.060
chiral volumes (Å^3)[d]		
C sp^3	0.158	0.200
C sp^2	0.163	0.220

Anisotropic Temperature Factors (U_{ij}) restraints	rmsd	target σ
DELU (Å^2)[e]	0.019	0.020
SIMU (Å^2)[e]	0.024	0.040
ISOR (Å^2)[e]	0.086	0.100

Mean Isotropic Equivalent B factor (Å^2)	
all protein atoms	11.48
main-chain atoms	9.81
side-chain atoms	12.92
water molecules	23.99
others	10.75
overall structure	13.50
core Ramachandran (%)[e]	87.4
H-bonds s.d.[f]	0.6
χ_1 pooled s.d.[f]	11.4
χ_2 pooled s.d.[f]	12.9
dihedral angles G factor[f]	−0.10

[a] $R_{cryst} = \sum_h |F_o - F_c| / \sum h F_o$, where F_o and F_c are the observed and calculated structure factor amplitudes of reflection h. [b] R_{free} is equal to R_{cryst} for a randomly selected 1.5% subset of reflections not used in refinement. [c] Assuming anisotropic B factors (nine parameters). [d] Values as reported by SHELX (*39*). [e] For the definition of DELU, SIMU, and ISOR restraints, see Materials and Methods. [f] Values as reported by PROCHECK (*42*).

an even anisotropic distribution in the structures, and the program PARVATI (*41*) was used to validate this distribution. The final round of refinement was carried out with the inclusion of all the data in the resolution range, yielding an R-free of 14.44% and an R-factor of 11.59%; the mean anisotropic distribution was 0.460.

Quality of the Models. The final model of rEDN includes all 135 amino acid residues with 17 side chains in alternate conformations, 1 acetate ion, and 226 water molecules with either full or partial occupancy. Over 87% of the residues in the structure are in the most favorable region of the Ramachandran plot as calculated by PROCHECK (*42*). The quality of the electron density maps is excellent for almost all the residues (Figure 2b), with the exception of a loop between residues 89−95. This loop is also seen to be highly disordered in the original 1.83 Å resolution structure (*18*) and in the 1.6 Å resolution structure (*19*), and this does not appear to depend on either the crystallization conditions or the temperature at which the diffraction data were collected. Interestingly, analogous regions from other ribonucleases (such as human Angiogenin (*43*) and the eosinophil cationic protein (*44*)) also show a high degree of flexibility in the same region of the molecule and invariably have poor electron density.

The overall structure is similar to the previously published 1.6 Å resolution structure of rEDN in complex with sulfate ions (PDB code 1HI2). The rms difference between the C^α atoms of the two structures is 0.33 Å, with most variation arising from the flexible loop region between residues 89−95. By eliminating this region from the rms calculation, the value drops to 0.23 Å. Even though the average B-factors of the present structure and 1HI2 are different (11.48 and 15.25 Å^2, respectively), the average isotropic B-factor distributions of the structures show similar profiles (Figure 3a). The region corresponding to the flexible loop shows the highest variation in an otherwise similar distribution.

Disordered Regions and Hydrogen Atoms. In the present structure, over 12% of the side chains (17 in total) were assigned alternate conformations. These discretely disordered residues are Phe5, Gln22, Asn25, Gln28, Ile30, Asn32, Asn53, Ser64, Arg68, Ile81, His82, Gln100, Met105, Val109, Asp112, His129, and Ile133. These residues are widely distributed over the surface of the molecule and are mostly polar or charged, the exceptions being Phe5, Ile30, Ile81, Met105, Val109, and Ile133. The disordered residues form several clusters within the structure. For example, residues Arg68, Asp112, and His129 are all situated within 6.0 Å of one another and have alternate conformations that are connected by tight water-mediated hydrogen-bonding networks. Similarly, both Asn25 and Gln100 are within 5 Å of Gln22 and show two distinct conformations that correlate with the alternate conformations of Gln22 (Figure 4a). A selection of other residues with alternate conformers is shown in Figure 4b.

Several hydrogen atoms were clearly visible in the electron density before their inclusion at riding positions in the refinement of the structure (Figure 2a). In a Fourier map analysis similar to the one previously reported for the RNase A structure at 0.87 Å resolution (*33*), positions of at least 290 out of a possible 915 hydrogen atoms included in refinement could be visualized at 1.5σ. However, the percentage of visible hydrogen atoms rises to greater than 60% if only hydrogen atoms attached to main-chain α carbons and nitrogens are considered. This is consistent with the fact that density peaks for hydrogen atoms are more easily discerned in the most ordered and rigid regions of the structure.

Active Site of EDN. All RNase A superfamily members contain the core active site subsites B_1, P_1, and B_2. These subsites accommodate the nucleotide bases located upstream (B_1) and downstream (B_2) of the scissile phosphodiester bond where cleavage of the RNA molecule takes place (P_1). These sites are well-conserved between RNase A and EDN, but the other, peripheral subsites responsible for binding the phosphodiester linkages upstream of B_1 and downstream of B_2 (P_0 and P_2, respectively) differ between these two proteins. In addition to these subsites, a new subsite (designated P_{-1}) has been identified in EDN (*19*, *45*). Unlike previous studies, the ultrahigh resolution of the present structure now enables us to describe the active site of EDN in minute detail.

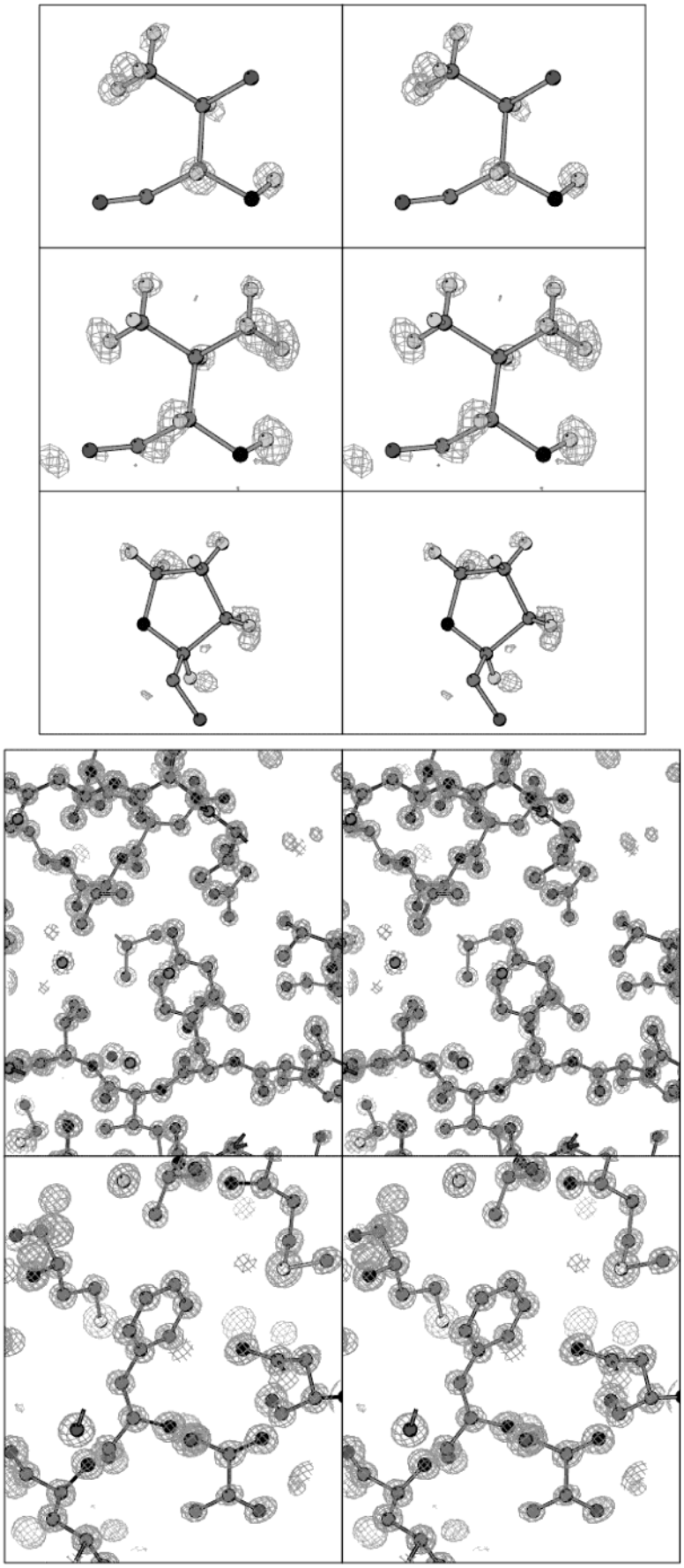

FIGURE 2: Electron density maps: (a) stereoviews of electron density for hydrogen atoms (light gray) around residues Thr13 (top), Val51 (middle), and Pro3 (bottom) as seen in F_o-F_c maps contoured at 3.0σ before the inclusion of hydrogens at riding positions during refinement, and (b) two views of the final $2F_o$-$F_{c\phi_{calc}}$ electron density maps showing the general quality of electron density around protein atoms when contoured at 3.3σ (top) and 3σ (bottom). Figure made using BOBSCRIPT (*64*).

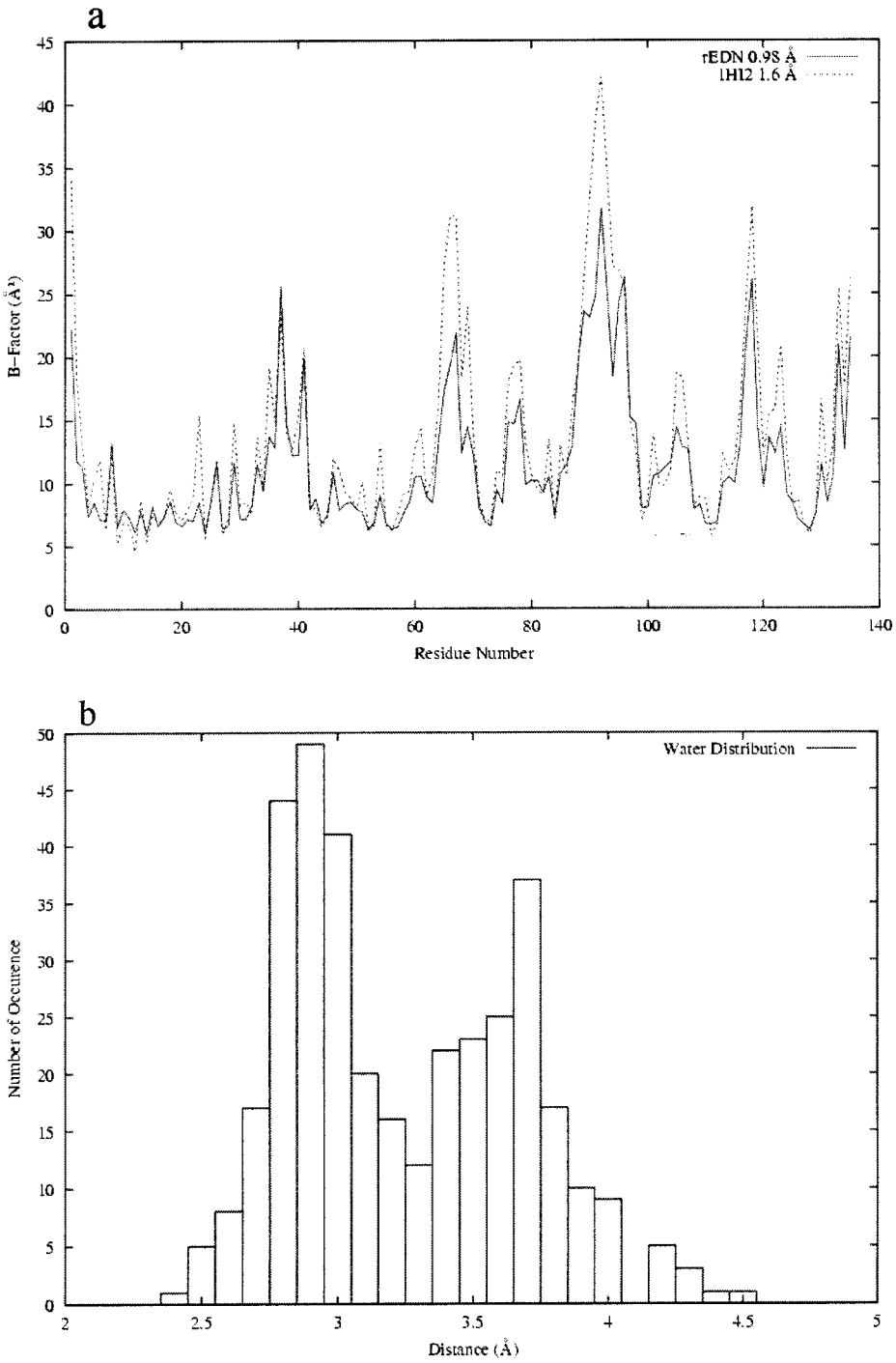

FIGURE 3: Analysis of isotropic B-factors and solvent organization. (a) Comparison of the residue-by-residue isotropic average B-factors in rEDN (solid lines) and 1HI2 (*19*) (dotted lines) shows a similar distribution of B-factors for both the structures. (b) Distribution of water molecules are plotted as a function of distance from the nearest protein atom in rEDN. The first water shell can be seen around 2.9 Å, and a second broader peak is seen around 3.7 Å.

P_1 Subsite. The P_1 site of EDN contains residues His15, Lys38, and His129 which form a triad that is conserved in all pancreatic-type ribonucleases studied so far; in RNase A, this triad consists of His12, Lys41, and His119. The P_1 site in the present structure was well-defined in the electron density map. The side chain of His15 was well-localized and could be visualized in $2F_o - F_c$ electron density maps to 7σ contour level. The mean isotropic displacement parameter for this side chain (7.06 Å^2) is among the lowest of any of the side chains of the structure. Similarly, Lys38 was clearly defined in the electron density map (Figure 5). In contrast, residue His129 has a much higher mobility (Figure 6a). In all RNase A structures reported so far, the side chain of the equivalent residue, His119, is found in one or both of two conformations (A and B with $\chi_1 \approx 150°$, $\chi_2 \approx 80°$, and $\chi_1 \approx -60°$, $\chi_2 \approx -70°$, respectively (*46*, *47*). Whereas conformation A is conducive to RNA-binding, conformation B is not (*48*, *49*). The latter conformation arises in low pH conditions or when polyvalent anions (such as phosphate or sulfate) or certain nucleotide inhibitors are present in the active site (*33*, *50*, *51*). In EDN, each of these conformations has been described for His129, depending on the presence

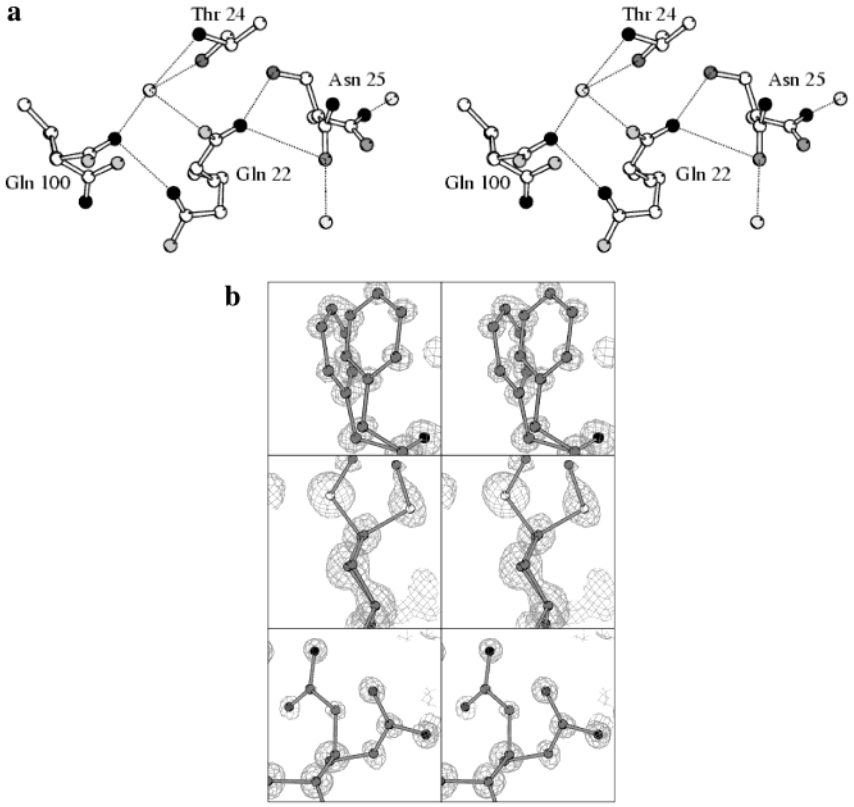

FIGURE 4: Discrete disorder in rEDN. (a) Correlated discrete disorder of Gln22, Asn25, and Gln100, indicating coordinated movement of these residues, is shown. All are situated within 5 Å of one another and are near the B_1 subsite. Water molecules (isolated spheres) stabilize both conformations of these residues by hydrogen-bond interactions (dashed lines). (b) Alternate conformations of selected residues is shown. Phe5 (top), Met105 (middle) and Gln22 (bottom) can be clearly seen in SigmaA weighted $2F_o$-F_c electron density maps contoured at the 2σ level. Figure made using BOBSCRIPT (*64*) and MOLSCRIPT (*65*).

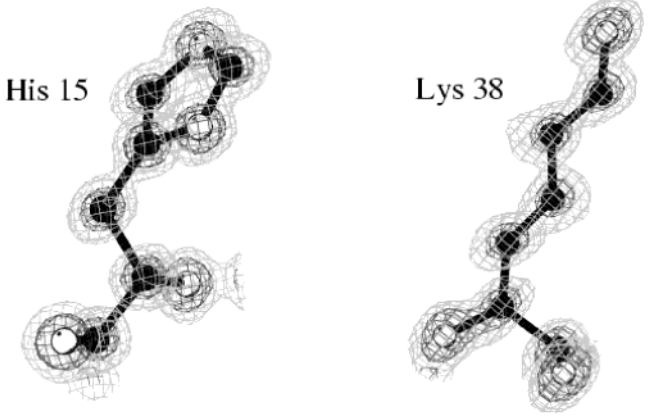

FIGURE 5: Quality of the $2F_o$-$F_{c\phi_{calc}}$ electron density maps for the P_1 subsite residues His15 (left) and Lys38 (right). The position of individual atoms can be clearly seen in maps contoured at 5σ (dark gray), here superimposed with the same maps contoured at 1σ (light gray).

or absence of different inhibitors or sulfate ions (*19*). In the present structure, His129 has two distinct conformations (Figure 6a). The first conformer adopts conformation A with $\chi_1 = 178°$ and $\chi_2 = 104°$, whereas the second conformer corresponds to conformation B with $\chi_1 = -72°$ and $\chi_2 = -66°$. The occupancies of these two conformations were refined to 0.60 and 0.40, respectively, by SHELX. In conformation A, the side chain of His129 is stabilized by a single water-mediated hydrogen bond between atom Nδ1 of histidine and atom Oδ2 of Asp131. In the previously reported structure of EDN in complex with sulfate (*19*), the side chain of His129 is maintained in conformation B by a hydrogen bond between atom Nδ1 of histidine and an oxygen atom from a sulfate ion. This interaction is absent in the present structure, and instead, conformation B is stabilized by hydrogen-bond interactions with a water molecule and the main-chain oxygen atom of residue Val128 (Figure 6b).

B_1 Subsite. The B_1 site of EDN consists of residues Thr42, Leu130, and Ile133, while the equivalent residues in RNase A have previously been identified as Thr45, Phe120, and Ser123. This site is important because it imparts the primary base specificity for RNA cleavage (*52*), which in the case of both RNase A and EDN is downstream of pyrimidine nucleotides. The residues corresponding to this site were clearly identified in the rEDN structure. In RNase A, the pyrimidine base makes numerous van der Waals contacts with Phe120, and hydrogen bonds with Thr45 (*25*) and, in some cases,with Asp83 (*21*). The position of Asp83 in EDN is occupied by His82. Through adoption of a side-chain orientation similar to conformation A of His129 ($\chi_1 = 165°$), this residue has previously been shown to be involved in van der Waals interactions with the adenine base when EDN is complexed with 5′-ADP (*19*). However, this nucleotide binds to EDN in an unconventional manner because adenine would be expected to bind at the B_2 subsite and not B_1. Interestingly, in the present unliganded structure, His82 is found to be flexible and is observed in two distinct conformations with $\chi_1 = 165°$, $\chi_2 = 68°$ (conformation A, occupancy = 0.66) and $\chi_1 = -67°$, $\chi_2 = -59°$ (conformation B, occupancy = 0.34), respectively (Figure 7a). In conformation A, His82 forms hydrogen bonds with Gln40 and

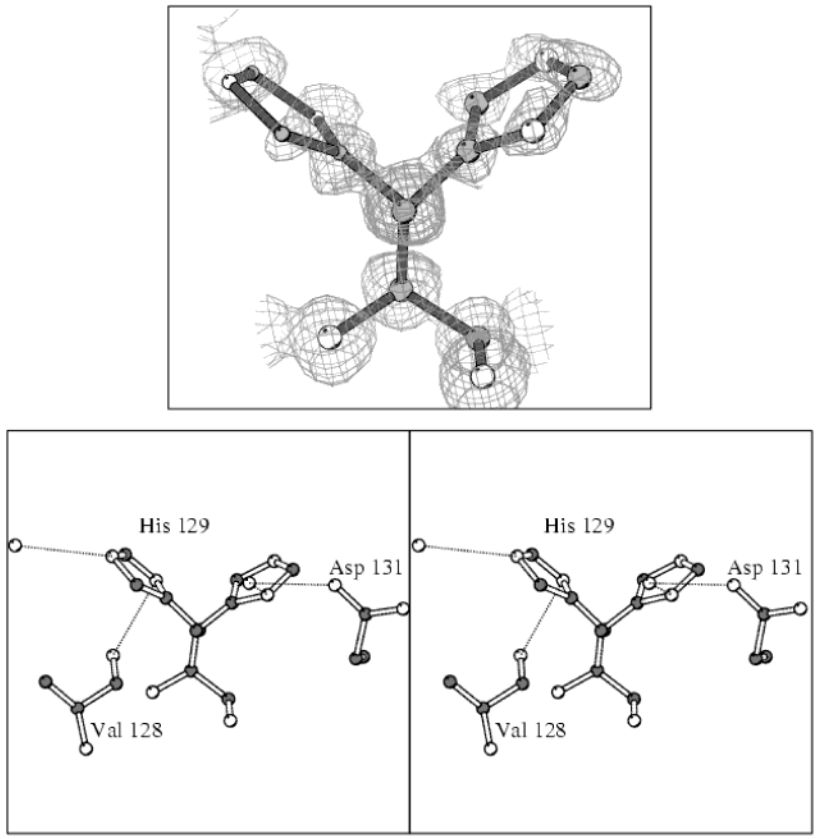

FIGURE 6: Catalytic residue His129 of the P_1 subsite. (a) His129 exists in both conformations (A and B) as seen in $2F_o$-F_c electron density maps contoured at the 1.5σ level. (b) Hydrogen-bond interactions (dashed lines) with neighboring residues and water molecules (white spheres) help to stabilize the alternate conformations of His129.

Asn84, whereas in conformation B, the only interactions are van der Waals interactions with Ile133 and Met105 (Figure 7b).

P_{-1} Subsite. In the original rEDN structure determined to a resolution of 1.83 Å (*18*), two sulfate ions were found to occupy distinct sites in the structure. The first sulfate was bound at the P_1 site and the other was bound at a site that had not been previously identified in other ribonucleases. This site was suggested to correspond to a P_{-1} phosphate-binding site. The presence of this site was later confirmed in the 1.6 Å resolution structure of rEDN·sulfate (*19*). This site is made up by residues Arg36, Asn39, and Gln40, but the region is only partly conserved in RNase A, being made up by Arg39, Pro42, and Val43. The sulfate ion bound at this site makes hydrogen-bond interactions with the side chain of Arg36 and main-chain atoms of Asn39 and Gln40. In the present structure, the Arg36 side chain is shifted by over 2.5 Å away from the position seen in the other EDN structures. The position potentially occupied by a sulfate ion is instead occupied by two water molecules that compensate by making hydrogen bonds with the main-chain atoms of Asn39 and Gln40 (Figure 8a).

B_2 Subsite. The B_2 subsite of EDN accommodates the nucleotide base downstream from the scissile phosphodiester bond and has been described in detail from structural studies on the binding of different adenylic nucleotide inhibitors (*19*). This site is made up by residues Arg68, Asn70, and Asp112 and is only partly conserved between EDN and RNase A. His119 also plays an important role in binding adenine by making van der Waals interactions with the base. This site has also been well characterized in RNase A by structural analysis of the complexes formed with different nucleotide-based inhibitors (*25*, *48*, *53*). The equivalent residues identified from these studies are Asn67, Gln69, Asn71, and Glu111. The conformations of all B_2 subsite residues in the present structure are similar to the previously reported 1.6 Å resolution structure of rEDN, with the exception of Arg68 and Asp112 that have two conformations here. In all published structures of EDN, these two residues occupy one or the other of these conformations, suggesting that these alternate conformations do not have any physiological significance but are merely indicative of the conformational freedom available to them. The alternate conformations of Arg68 and Asp112 are involved in hydrogen bonds with neighboring water molecules.

*P_0 and P_2 Subsites.*The P_0 and P_2 subsites are involved in binding the phosphodiester linkages upstream of B_1 and downstream of B_2, respectively. In RNase A, these roles are played by Lys66 (P_0), Lys7 (P_2), and Arg10 (P_2) (*23*, *24*, *26*). In EDN, these sites are not conserved and are represented by Ser64, Trp7, and Trp10 which are not likely to bind phosphate. Ser64 exists in two conformations in the present structure, with one conformation similar to that seen in the 1.6 Å resolution structure. Trp7 is one of only two tryptophan residues in EDN, the other being Trp10 and forming part of the Trp-X-X-Trp motif known to be the signal for a unique C-mannosylation modification on Trp7 (*16*, *17*). Trp7 has much higher average isotropic B-factors for its side chain (16.1 Å^2) than does Trp10 (8.4 Å^2), indicating the increased availability of conformational space for the former amino acid to allow it to bind the carbohydrate moiety.

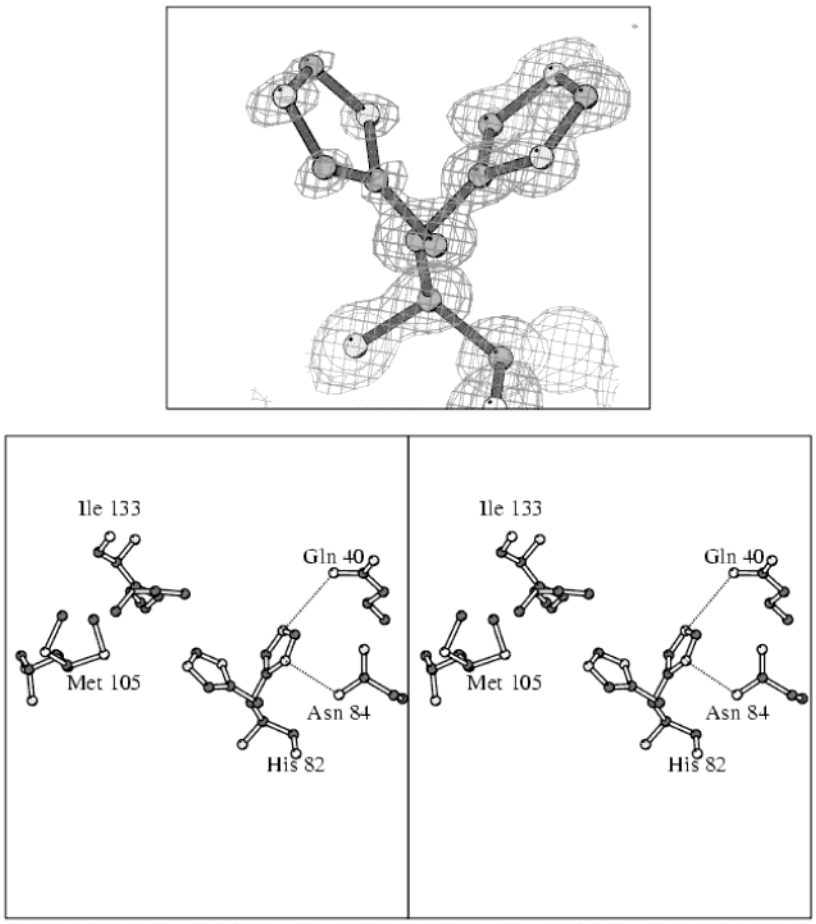

FIGURE 7: Residue His82 in vicinity of the B_1 subsite. (a) His82 shows two distinct conformers similar to conformations A and B of His129. The electron density map is contoured at 1σ. (b) Stereoview of molecular interactions between His82 and neighboring residues is shown. In conformation A, His82 forms hydrogen-bond interactions (dashed lines) with Asn84 and Gln40. In conformation B, only van der Waals interactions with Met105 and Ile133 stabilize the conformation.

Solvent Structure. A total of 227 water molecules were included in the rEDN structure: 182 were refined with full occupancy and 45 were refined with half occupancy on the basis of the quality of electron density. In addition to these solvent molecules, a well-defined acetate ion from the crystallization medium was also identified in the model. The high resolution of the model allows for a detailed analysis of solvent molecules identified in the structure. The crystals have a solvent content of 40.02% (v/v), which translates to a volume of 51 685 Å^3 occupied by waters in the unit cell. This value corresponds to a theoretical number of 1720 waters in the unit cell or 430 fully occupied water molecules per asymmetric unit. Hence, the fully occupied solvent molecules account for at least 43% of the total water content in the unit cell. Taking into account the space occupied by protein alternate conformations, solvent ions and partially occupied water molecules, this number can be estimated to be as high as 52.7%. The solvent molecules are well ordered with an average isotropic B factor of 24 Å^2 for the water molecules and 10.7 Å^2 for the acetate ion. The trend in B-factor values is well-correlated with the number of protein contacts and decreases from 27 Å^2 for one contact to 25 Å^2 for two, 22 Å^2 for three, and 20.75 Å^2 for four contacts.

The high resolution of the structure also allows for the identification of solvent sites situated far away from the protein surface. Contact analysis was used to segregate water molecules into different hydration shells (*54*). Water molecules were grouped into the first hydration shell if they made at least one hydrogen bond with a protein atom. They were assigned into the second hydration shell if they only interacted with other water molecules. By using these criteria and a hydrogen-bond cutoff distance of 3.3 Å, 152 water molecules were identified in the first hydration shell and 72 in higher shells. The distribution of water sites as a function of distance from the nearest protein atom is shown in Figure 3b. The first shell is well-defined at 2.8 Å, with a second, broader peak at 3.7 Å. These results are comparable to that seen for the atomic resolution structure of RNase A (*33*).

An analysis of water interactions with protein atoms shows that there are 2.53 times more hydrogen-bond interactions with main-chain oxygen atoms (76) than there are with main-chain nitrogen atoms (30). By comparison, the number of hydrogen bonds made with side-chain oxygen atoms (88) is only around twice the number made with side-chain nitrogen atoms (47). These results are in keeping with previous statistical and simulation studies, which suggest that main-chain oxygen atoms have a greater ability than side-chain oxygen atoms to form hydrogen bonds with water molecules (*55*).

DISCUSSION

The crystal structure of rEDN at 0.98 Å resolution reported here is the highest reported for this protein. This structure

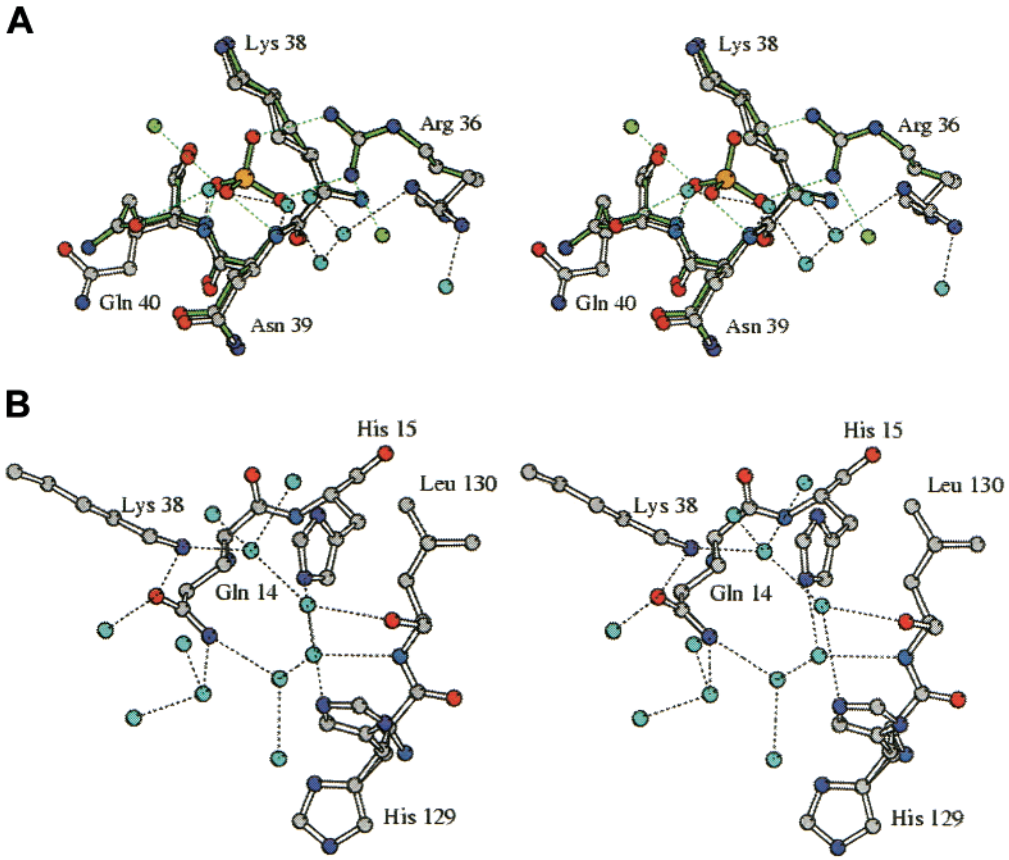

FIGURE 8: (a) P_{-1} subsite of rEDN in the presence or absence of sulfate ion is shown. In the presence of sulfate ion, as previously described (PDB Code 1HI2) (*19*), residues Arg36 and Gln40 make direct hydrogen-bonded contact with sulfate oxygen atoms (green sticks and dashed lines). In the sulfate-free rEDN structure, these residues point away from the binding site, and the position occupied by sulfate in the complex is now occupied by a network of water molecules (cyan) forming hydrogen bonds (black dashed lines). (b) Water networks around the P_1 subsite of rEDN are shown. These networks help to maintain the structure of active site residues His15, Lys38, and His129.

joins a select group of ribonuclease structures determined at atomic resolution (*32*, *33*).

It is well-documented that the P_1 subsite catalytic residue His129 (His119 in RNase A) can adopt one of two preferential side-chain conformations. With RNase A, one of these conformations (B) is favored at low pH or when certain nucleotide-based inhibitors or polyvalent anions such as sulfate are present in the active site, whereas the other (A) is compatible with RNA-binding (*50*, *56*). With rEDN, complex formation with sulfate ions or nucleotide-based inhibitors likewise leads to the adoption of one or the other of these conformations (*19*). In the present study, His129 adopts both the possible conformations, each being stabilized by hydrogen bonds with solvent and protein atoms (Figure 6b). This clearly represents the inherent flexibility of His129. The other residues of the P_1 catalytic center (His15 and Lys38) are very well-defined in the electron density maps and do not have disorder (Figure 5).

The B_1 subsite of rEDN shares modest similarity with that of RNase A. In rEDN, this subsite is predicted to contain a histidine residue (His82) that shows two conformations in the present structure (Figure 7). These are similar to those seen for His129 and have χ_1 and χ_2 angles corresponding to conformations A and B. Although there is currently no direct evidence demonstrating a role for His82 in the B_1 subsite, these conformational variations seem to imply that the binding of a nucleotide at this site could influence the side-chain conformation as seen for His129 in the P_1 subsite (*19*).

The high resolution of the present structure makes it possible to describe the recently identified P_{-1} subsite of rEDN in the absence of sulfate ions. This site is made up of residues Arg36, Asn39, and Gln40, each of which can make hydrogen-bond interactions with sulfate oxygen atoms. In the absence of sulfate ions, the Arg36 side chain moves away from the binding pocket and forms water-mediated hydrogen bonds with Asn39 near the P_1 subsite (Figure 8a). Hence, in the present crystals, the P_{-1} site is not clearly defined. This suggests that the binding of a nucleotide or sulfate ion leads to a restructuring of the region to form the P_{-1} subsite.

Clusters of residues displaying correlated side-chain disorder were seen in the rEDN structure, with correlated conformations extending over 3−5 residues (Figure 4a). The presence of disorder correlated over 5−8 Å suggests that motion of residues appreciably occurs in coordinated groups rather than in isolation. Such patterns of disorder have also been seen in atomic resolution structures of crambin (*57*, *58*) and the Col1E1 repressor of primer (ROP) protein (*59*).

Water molecules play an important role in maintaining the structural stability of proteins. The present structure has revealed the extensive water-mediated hydrogen-bond networks that maintain the active site subsites of rEDN (Figure 8b). In addition, it has been possible to discriminate between water molecules that bind directly to the protein and those that only hydrogen bond with other water molecules (Figure 2b). The average hydrogen-bond distance decreases from

2.96 Å for protein-water contacts to 2.90 Å for water−water contacts. This trend is similar to that seen in other atomic resolution protein structures (*33*, *60*).

The sequences of EDNs from at least nine primate species have been described (*61*). The primary sequence identity among these EDNs is only about 60%, because these are among the most rapidly evolving functional coding sequences known (*62*). Despite this divergence, residues forming the catalytic triad (P_1) and the P_{-1} subsite are absolutely conserved, and residues comprising the B_2 subsite are structurally conserved. However, His82 and Ile133 (both predicted to be part of the B_1 subsite) are not conserved in all primates. For EDN sequences derived from tamarin and owl monkey (GenBank accession numbers U24099 and U88827, respectively), these residues are instead present as tyrosine and threonine, respectively. These substitutions may impart differences in substrate specificity, although in the absence of structural data describing the mode of pyrimidine binding at the B_1 subsite of EDN, their significance is unclear.

The present structure of rEDN represents a significant improvement in the structural model available for this protein. The product of all the disordered residues seen in the model likely accounts for all the possible discrete conformational preferences of the protein. The subsite structures have been described in detail and we have identified those key active site residues that display side-chain flexibility and those that are rigid. In particular, the discrete disorder in His82 suggests that this residue could play an important part in binding nucleotides at the B_1 site. These results will aid greatly in the design of inhibitors to combat symptoms associated with overexposure to EDN in eosinophil-mediated inflammation and hypereosinophilic disease states.

ACKNOWLEDGMENT

We thank Drs. Richard Youle, Robert Prill, Motoshi Suzuki at NINDS, Bethesda, MD, for the generous gift of rEDN used in this study. We are grateful to the staff at the Synchrotron Radiation Source, Daresbury, U.K., for help with X-ray data collection. We also thank members of the Structural Biology Group for the constructive criticism of the manuscript.

REFERENCES

1. Rosenberg, H. F., Tenen, D. G., and Ackerman, S. J. (1989) *Proc. Natl. Acad. Sci. U.S.A. 86*, 4460−4464.
2. Beintema, J. J., Schuller, C., Irie, M., and Carsana, A. (1988) *Prog. Biophys. 51*, 165−192.
3. Ackerman, S. J., Loegering, D. A., Venge, P., Olsson, I., Harley, J. B., Fauci, A. S., and Gleich, G. J. (1983) *J. Immunol. 131*, 2977−2982.
4. Sierakowska, H., and Shugar, D. (1977) *Prog. Nucleic Acid Res. Mol. Biol. 20*, 59−130.
5. Gleich, G. J., Kita, H., and Adolphson, C. R. (1995) in *Samter's Immunologic Diseases* (Frank, M. M., Austen, K. F., Claman, H. N., and Unanue, E. R., Eds.) pp 205−245, Little, Brown & Co., Boston, MA.
6. Hamann, K. J., Barker, R. L., Loegering, D. A., and Gleich, G. J. (1987) *J. Parasitol. 73*, 523−529.
7. Domachowske, J. B., Dyer, K. D., Bonville, C. A., and Rosenberg, H. F. (1998) *J. Infect. Dis. 177*, 1458−1464.
8. Fredens, K., Dahl, R., and Venge, P. (1982) *J. Allergy Clin. Immunol. 70*, 361−366.
9. Gleich, G. J., Loegering, D. A., Bell, M. P., Checkel, J. L., Ackerman, S. J., and McKean, D. J. (1986) *Proc. Natl. Acad. Sci. U.S.A. 83*, 3146−3150.
10. Gleich, G. J., and Adolphson, C. R. (1986) *Adv. Immunol. 39*, 177−253.
11. Durack, D. T., Ackerman, S. J., Loegering, D. A., and Gleich, G. J. (1981) *Proc. Natl. Acad. Sci. U.S.A. 78*, 5165−5169.
12. Rosenberg, H. F. (1998) *Cell. Mol. Life Sci. 54*, 795−803.
13. Newton, D. L., Walbridge, S., Mikulski, S. M., Ardelt, W., Shogen, K., Ackerman, S. J., Rybak, S. M., and Youle, R. J. (1994) *J. Neurosci. 14*, 538−544.
14. Sorrentino, S., Glitz, D. G., Hamann, K. J., Loegering, D. A., Checkel, J. A., and Gleich, G. J. (1992) *J. Biol. Chem. 267*, 14859−14865.
15. Slifman, N. R., Leogering, D. A., McKean, D. J., and Gleich, G. J. (1986) *J. Immunol. 137*, 2913−2917.
16. Hofsteenge, J., Muller, D. R., de Beer, T., Loffler, A., Richter, W. J., and Vliegenthart, J. F. G. (1994) *Biochemistry 33*, 13524−13530.
17. Krieg, J., Hartmann, S., Vicentini, A., Glasner, W., Hess, D., and Hofsteenge, J. (1998) *Mol. Biol. Cell 9*, 301−309.
18. Mosimann, S. C., Newton, D. L., Youle, R. J., and James, M. N. G. (1996) *J. Mol. Biol. 260*, 540−552.
19. Leonidas, D. D., Boix, E., Prill, R., Suzuki, M., Turton, R., Minson, K., Swaminathan, G. J., Youle, R. J., and Acharya, K. R. (2001) *J. Biol. Chem. 276*, 15009−15017.
20. Boix, E., Nikolovski, Z., Moiseyev, G. P., Rosenberg, H. F., Cuchillo, C. M., and Nogués, M. V. (1999) *J. Biol. Chem. 274*, 15605−15614.
21. Raines, R. T. (1998) *Chem. Rev. 98*, 1045−1065.
22. Nogués, M. V., Moussaoui, M., Boix, E., Vilanova, M., Ribó, M., and Cuchillo, C. M. (1998) *Cell. Mol. Life Sci. 54*, 766−774.
23. Boix, E., Nogués, M. V., Schein, C. H., Benner, S. A., and Cuchillo, C. M. (1994) *J. Biol. Chem. 269*, 2529−2534.
24. Fisher, B. M., Grilley, J. E., and Raines, R. T. (1998) *J. Biol. Chem. 273*, 34134−34138.
25. Fontecilla-Camps, J. C., de Llorens, R., le Du, M. H., and Cuchillo, C. M. (1994) *J. Biol. Chem. 269*, 21526−21531.
26. Richardson, R. M., Parés, X., and Cuchillo, C. M. (1990) *Biochem. J. 267*, 593−599.
27. Witzel, H., and Barnard, E. A. (1962) *Biochem. Biophys. Res. Commun. 7*, 295−299.
28. Richards, F. M., and Wyckoff, H. W. (1971) in *The Enzymes* (Boyer, P. D., Ed.) pp 647−806, Academic Press, New York.
29. Sheldrick, G. M. (1990) *Acta Crystallogr. A46*, 467−473.
30. MacArthur, M. W., and Thornton, J. M. (1999) *Acta Crystallogr. D55*, 994−1004.
31. Berman, H. M., Westbrook, J., Feng, Z., Gilliland, G., Bhat, T. N., Weissig, H., Shindyalov, I. N., and Bourne, P. E. (2000) *Nucleic Acid Res. 22*, 235−242.
32. Sevcik, J., Dauter, Z., Lamzin, V. S., and Wilson, K. S. (1996) *Acta Crystallogr. D52*, 327−344.
33. Esposito, L., Vitagliano, L., Sica, F., Sorrentino, G., Zagari, A., and Mazzarella, L. (2000) *J. Mol. Biol. 297*, 713−732.
34. Wilson, A. J. C. (1942) *Nature 150*, 151−152.
35. Brünger, A. T., Adams, P. D., Clore, G. M., DeLano, W. L., Gros, P., Grosse-Kunstleve, R. W., Jiang, J. S., Kuszewski, J., Nilges, M., Pannu, N. S., Read, R. J., Rice, L. M., Simonson, T., and Warren, G. L. (1998) *Acta Crystallogr. D54*, 905−921.
36. Brünger, A. T. (1992) *Nature 355*, 472−475.
37. Brünger, A. T., Krukowski, J., and Erickson, J. (1990) *Acta Crystallogr. A46*, 585−593.
38. Jones, T. A., Zou, J. Y., Cowan, S. W., and Kjeldgaard, M. (1991) *Acta Crystallogr. A47*, 110−119.
39. Sheldrick, G. M., and Schneider, T. R. (1997) *Methods Enzymol. 277*, 319−343.
40. Engh, R. A., and Huber, R. (1991) *Acta Crystallogr. A47*, 392−400.
41. Merrit, E. A. (1999) *Acta Crystallogr. D55*, 1109−1117.
42. Laskowski, R. A., MacArthur, M. W., Moss, D. S., and Thornton, J. M. (1993) *J. Appl. Crystallog. 26*, 283−291.

43. Leonidas, D. D., Shapiro, R., Allen, S. C., Subbarao, G. V., Veluraja, K., and Acharya, K. R. (1999) *J. Mol. Biol. 285*, 1209−1233.
44. Boix, E., Leonidas, D. D., Nikolovski, Z., Nogués, M. V., Cuchillo, C. M., and Acharya, K. R. (1999) *Biochemistry 38*, 16794−16801.
45. Mosimann, S. C., Ardelt, W., and James, M. N. G. (1994) *J. Mol. Biol. 236*, 1141−1153.
46. Borkakoti, N. (1983) *Eur. J. Biochem. 132*, 89−94.
47. deMel, V. S. J., Martin, P. D., Doscher, M. S., and Edwards, B. F. P. (1992) *J. Biol. Chem. 267*, 247−256.
48. Zegers, I., Maes, D., Dao-Thi, M.-H., Poortmans, F., Palmer, R., and Wyns, L. (1994) *Protein Sci. 31*, 2322−2339.
49. Leonidas, D. D., Shapiro, R., Irons, L. I., Russo, N., and Acharya, K. R. (1997) *Biochemistry 36*, 5578−5588.
50. Fedorov, A. A., Joseph-McCarthy, D., Fedorov, E., Sirakova, D., Graf, I., and Almo, S. C. (1996) *Biochemistry 35*, 15962−15979.
51. Berisio, R., Lamzin, V., Sica, F., Wilson, K. S., Zagari, A., and Mazzarella, L. (1999) *J. Mol. Biol. 292*, 845−854.
52. McPherson, A., Brayer, G., Cascio, D., and Williams, R. (1986) *Science 2*, 765−768.
53. Toiron, C., Gonzalez, C., Bruix, M., and Rico, M. (1996) *Protein Sci. 5*, 1633−1647.
54. CCP4 (1994) *Acta Crystallogr. D50*, 760−763.
55. Thanki, N., Thornton, J. M., and Goodfellow, J. M. (1988) *J. Mol. Biol. 202*, 637−657.
56. Gilliland, G. (1997) in *Ribonucleases: Structures and functions.* (D'Alessio, G., and Riordan, J. F., Eds.) pp 305−341, Academic Press, Inc., New York.
57. Teeter, M. M., Roe, S. M., and Heo, N. H. (1993) *J. Mol. Biol. 230*, 292−311.
58. Yamano, A., and Teeter, M. M. (1994) *J. Mol. Biol. 269*, 13956−13965.
59. Vlassi, M., Dauter, Z., Wilson, K. S., and Kokkinidis, M. (1998) *Acta Crystallogr. D54*, 1245−1260.
60. Kumaraswamy, V. S., Lindley, P. F., Slingsby, C., and Glover, I. D. (1996) *Acta Crystallogr. D52*, 611−622.
61. Rosenberg, H. F., and Domachowske, J. B. (2001) *Methods Enzymol. 341*, 273−286.
62. Rosenberg, H. F., Dyer, K. D., Tiffany, H. L., and Gonzalez, M. (1995) *Nat. Genet. 10*, 219−223.
63. French, S., and Wilson, K. S. (1978) *Acta Crystallogr. A34*, 517−525.
64. Esnouf, R. M. (1997) *J. Mol. Graphics 15*, 132−134.
65. Kraulis, P. J. (1991) *J. Appl. Crystallogr. 24*, 946−950.

BI015911F